Cell Reports

Article

The non-specific matrix thalamus facilitates the cortical information processing modes relevant for conscious awareness

Graphical abstract

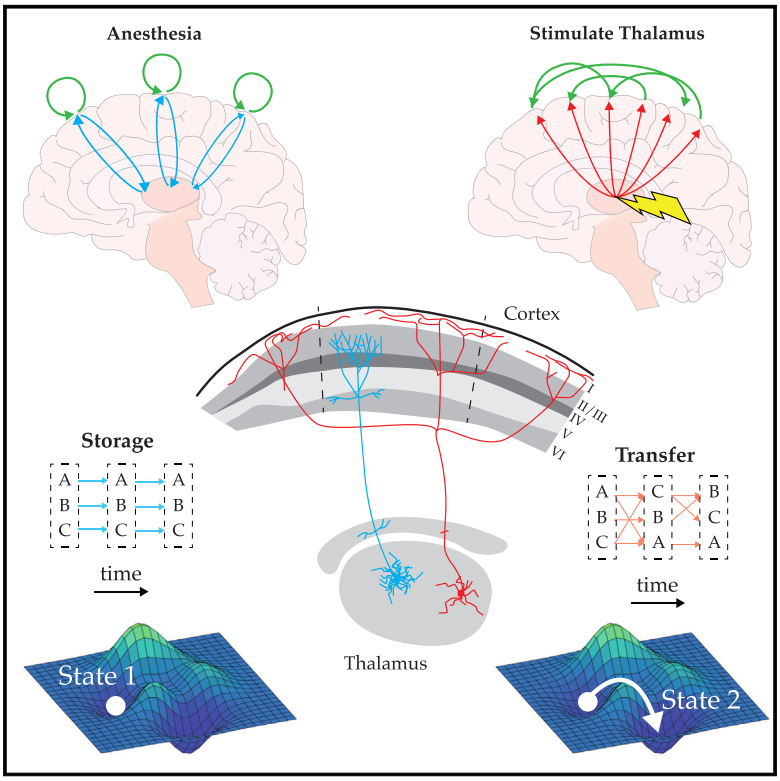

Authors

Eli J. Müller, Brandon R. Munn, Michelle J. Redinbaugh, Joseph Lizier, Michael Breakspear, Yuri B. Saalmann, James M. Shine

Correspondence

eli.muller@sydney.edu.au

In brief

Muller et al. develop a large-scale biophysical corticothalamic model imbued with diffusely projecting matrix thalamic nuclei and show that stimulation of these cells facilitates recovery of consciousness following propofol anesthesia—recapitulating empirical observations in macaque monkeys. The authors further show how the matrix thalamus augments cortical attractors and promotes modes of high information transfer.

Highlights

- Corticothalamic system imbued with matrix thalamus captures key features of consciousness
- Matrix stimulation recovers consciousness under propofol recapitulating macaque observation
- Matrix nuclei modulate cortical attractors facilitating modes of high information transfer

Müller et al., 2023, Cell Reports *42*, 112844
August 29, 2023 © 2023 The Authors.
https://doi.org/10.1016/j.celrep.2023.112844

CellPress

Cell Reports

CellPress
OPEN ACCESS

Article

The non-specific matrix thalamus facilitates the cortical information processing modes relevant for conscious awareness

Eli J. Müller,[1,2,5,7,*] Brandon R. Munn,[1,2] Michelle J. Redinbaugh,[3] Joseph Lizier,[2,5] Michael Breakspear,[6] Yuri B. Saalmann,[3,4] and James M. Shine[1,2]

[1]Brain and Mind Centre, The University of Sydney, Sydney, NSW, Australia
[2]Centre for Complex Systems, The University of Sydney, Sydney, NSW, Australia
[3]Department of Psychology, University of Wisconsin-Madison, Madison, WI, USA
[4]Wisconsin National Primate Research Centre, Madison, WI, USA
[5]School of Computer Science, The University of Sydney, Sydney, NSW, Australia
[6]The University of Newcastle, Newcastle, NSW, Australia
[7]Lead contact
*Correspondence: eli.muller@sydney.edu.au
https://doi.org/10.1016/j.celrep.2023.112844

SUMMARY

The neurobiological mechanisms of arousal and anesthesia remain poorly understood. Recent evidence highlights the key role of interactions between the cerebral cortex and the diffusely projecting matrix thalamic nuclei. Here, we interrogate these processes in a whole-brain corticothalamic neural mass model endowed with targeted and diffusely projecting thalamocortical nuclei inferred from empirical data. This model captures key features seen in propofol anesthesia, including diminished network integration, lowered state diversity, impaired susceptibility to perturbation, and decreased corticocortical coherence. Collectively, these signatures reflect a suppression of information transfer across the cerebral cortex. We recover these signatures of conscious arousal by selectively stimulating the matrix thalamus, recapitulating empirical results in macaque, as well as wake-like information processing states that reflect the thalamic modulation of large-scale cortical attractor dynamics. Our results highlight the role of matrix thalamocortical projections in shaping many features of complex cortical dynamics to facilitate the unique communication states supporting conscious awareness.

INTRODUCTION

Consciousness is defined as the capacity to be aware of and responsive to one's external environment and internal states.[1] Despite a pervasive interest that extends beyond the scientific community, our understanding of the biological mechanisms that support conscious awareness remains incomplete. Many different properties of whole-brain neuroimaging data have been linked to alterations in the level of consciousness,[2–5] typically as a function of anesthetic manipulation.[2] Despite these advances, we lack a systems-level description of how consciousness emerges from neurobiology.

There has been a long-standing appreciation that interactions of the thalamocortical system are crucial for conscious awareness.[6–12] Recent evidence has reinforced this hypothesis while incorporating additional biological complexity. For instance, the administration of several classes of anesthetic agents blocks the intracompartment coupling of thick-tufted layer 5 (L5) cortical pyramidal neurons, which in turn are under the influence of diffusely projecting[13,14] matrix thalamic nuclei.[15] Experimental work in macaques has demonstrated that propofol anesthesia induces a reduction of coordinated activity between the thalamus and deep cortical layers (including those that house the cell bodies of L5 pyramidal neurons) across multiple cortical areas.[16] Furthermore, electrically stimulating the central thalamus restores the coherent activity that is diminished during anesthetic-induced loss of consciousness and facilitates recovery of consciousness.[16–18] Another thalamic stimulation study in anesthetized macaque showed that recovery of consciousness was concomitant with a broad evoked response spanning many cortical areas and an increase in corticocortical connectivity.[17] These results suggest a crucial role of the interactions between the diffusely projecting matrix thalamus and L5 pyramidal neurons for consciousness.[8,9,19,20] However, challenges inherent in recording sufficiently large numbers of neurons across a broad range of behavioral states limit the capacity to determine the precise systems-level importance of these interactions.

Computational modeling allows simulation of large-scale neural systems and hence offers a unique approach to this problem.[21–23] Here, we augment a well-validated neural mass model of the corticothalamic system[24] with neurobiological details specific to the present question: namely, both targeted and diffuse

This is an open access article under the CC BY-NC-ND license (http://creativecommons.org/licenses/by-nc-nd/4.0/).

Table 1. Corticothalamic neural mass parameters

Parameter	Description	Value	Unit
γ_e	cortical damping rate	116	s^{-1}
Q^{max}	maximum firing rate	340	s^{-1}
θ	firing threshold	12.9	mV
σ'	threshold spread	3.8	mV
φ_n	input noise amplitude spectral density	1×10^{-5}	s^{-1}
α	decay rate of cell-body potential	83	s^{-1}
β	rise rate of cell-body potential	769	s^{-1}
ν_{ee}	intranode coupling strengths	1.5	mV s
ν_{ei}		−3	mV s
ν_{es_c}		0.57	mV s
ν_{se}		3.4	mV s
ν_{s_cr}		−1.5	mV s
ν_{s_cn}		3.6	mV s
ν_{re}		0.17	mV s
ν_{rs_c}		0.05	mV s
$\tau_{es_c,es_m} + \tau_{s_ce,s_me}$	corticothalamic loop delay	85	ms

Adapted from Abeysuriya et al.[33]

thalamocortical populations,[13,14] empirically derived thalamocortical coupling gradients,[25] and a neurobiological implementation of propofol-mediated anesthesia.[26] We interrogate this corticothalamic model's role in generating key features of the anesthetic state and the mechanisms recovering systems-level signatures of arousal following selective stimulation of the matrix thalamus. From there, we exploit the glass-box nature of our model to quantify thalamic contributions to shaping cortical dynamics and systems-level modes of information processing. Together, this approach provides a working model of whole-brain dynamics across arousal states.

RESULTS

Whole-brain model of corticothalamic interactions

We simulated a network of 400 corticothalamic neural masses (from a widely employed parcellation scheme[27]) using the neural field simulation software *nftSim*.[28] A neural mass model is a mathematical description of a population of neurons that incorporates their biophysical properties, but rather than tracking single-neuron activity, it approximates neuronal firing rates using parametric probability distributions, which change over time. This approach rests on a key assumption—the diffusion approximation—which states that for a large population of neurons with sufficiently weak correlations between neurons, the dynamics of the first two moments (i.e., the mean and variance) are sufficient to describe population-level behavior.[22,29–32] Furthermore, the variance can be assumed to be static, which means that the mean dynamics of the firing rate distribution (which aggregates synaptic inputs and all stochastic effects) can be systematically analyzed. Interactions between each population's mean firing rate can further be parameterized to capture timescales of response and propagation, as well as average between-population couplings. The parameters for each corticothalamic neural mass used in the present model are set to "eyes-closed" estimates based on Bayesian fits to a power spectrum of human electrophysiological recordings[33] (see Table 1). This yields activity with a characteristic 1/f spectrum and a peak in the alpha frequency band (8–13 Hz). These oscillatory rhythms capture spike rate modulations of neurons across a population that relate to extracellular field potentials measured via electroencephalogram (EEG) and local field potential (LFP) recordings.[34]

In line with empirical observation,[35–38] corticocortical connectivity was modeled as a combination of exponential spatial drop-off (i.e., connection density decreasing exponentially with interareal geodesic distance), with symmetric coupling of homologous areas between hemispheres, and connectivity strength estimated from empirical measures of white-matter fiber density.[39] To mimic the known excitatory interactions between the matrix thalamus and L5 pyramidal neurons,[40] we leveraged previous work that identified core (specific) and matrix (non-specific) thalamocortical nuclei through genetic expression and investigated their temporal coordination with regions spread across the cerebral cortex.[25]

We first optimized the global scaling of corticocortical connectivity to generate correlations between cortical areas that are consistent with empirical observations[41,42] (Figure 1F). Left unchecked, these excitatory interactions manifest runaway activity; however, this does not typically occur in practice due to a key feature of the cerebral cortex—tight excitatory-inhibitory (E-I) balance.[43] In line with previous work,[41,44] we impose an E-I balance by upscaling local inhibition to ensure a 3 Hz steady-state firing rate attractor for the cortical populations, consistent with *in vivo* recordings.[45] Since the matrix thalamus is exclusively excitatory, activity in the matrix thalamus acts to break E-I cortical balance and hence weaken the stability of cortical attractors imposed by this E-I balance, resulting in a heterogeneous spread of cortical firing rates.

We optimized global structural connectivity scaling by comparing the correlation matrix of model outputs with functional connectivity calculated on empirical 7T resting-state fMRI data ($r = 0.44, p < 10^{-16}$; Figure 1F).[42,46] Having imposed a baseline wake state for the model, we next interrogated the systems-level features of propofol anesthesia.[16]

Modeling propofol anesthesia

Although the precise mechanisms are not well understood, the majority of anesthetic agents up-regulate the activity of inhibitory gamma-aminobutyric acid ($GABA_A$) receptors,[47] causing a prolongation of the inhibitory post-synaptic response potentials (IPSPs), an integral parameter in our neural field model.[21] To capture this up-regulation under propofol anesthesia, we followed recent work[26] and introduced a parameter, ρ (Figure 1G), which scales all IPSPs in the model while maintaining a fixed peak response (see STAR Methods). This is consistent with recent work showing that explicit anesthetic effects on thalamocortical projections include decoupling of evoked-response potentials in apical dendrites from somatic dynamics in L5 cortical pyramidal neurons.[15] To prevent a potential corticocentric

CellPress
OPEN ACCESS

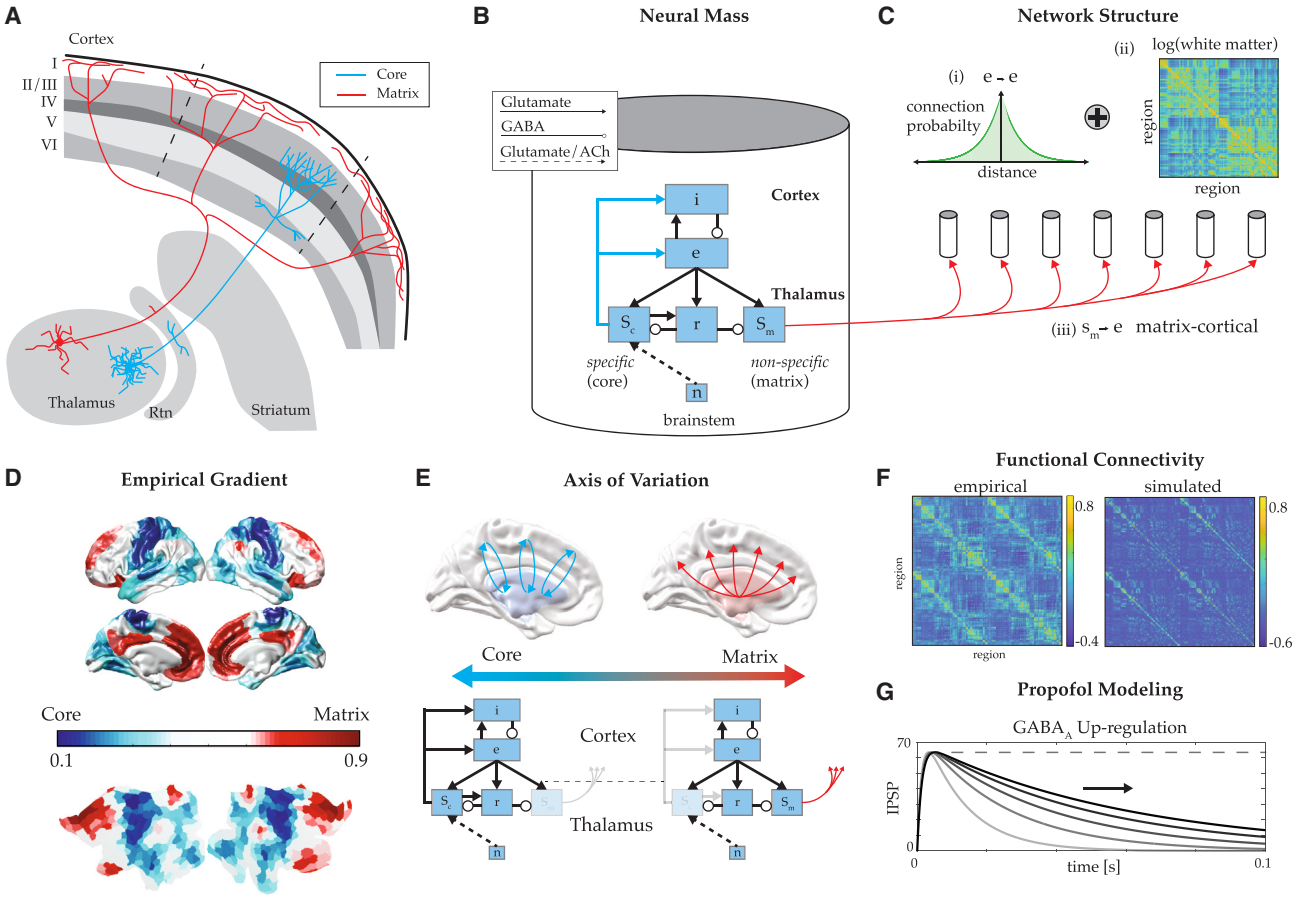

Figure 1. Distinct thalamocortical subtypes and whole-brain modeling

(A) Schema of characteristic projection profiles of core (specific) and matrix (non-specific) thalamocortical neurons (adapted from Clascá et al.[13]).

(B) Corticothalamic neural mass—the cerebral cortex consists of an excitatory population (*e*) and an inhibitory population (*i*), the thalamus consists of a core population (*Sc*) describing targeted thalamocortical projections, and a matrix population (*Sm*) describing diffuse thalamocortical projections; subcortical drive from the brainstem (*n*).

(C) Network structure combines corticocortical exponential drop-off (i) and empirical white-matter estimates (ii) and thalamocortical matrix "one-to-all" connectivity (iii).

(D) Cortical topography of thalamic subtype projections inferred from human gene expression data detailing calcium-binding proteins unique to each.[25]

(E) The extent of each thalamic population's interaction with the cerebral cortex was tuned to match the observed empirical gradient.[25]

(F) Comparison of functional connectivity for the model and resting-state fMRI data showed a robust positive correlation ($r = 0.44, p < 10^{-16}$).

(G) Propofol is modeled as a $GABA_A$ up-regulation that increases net inhibition through the prolongation of the timescale of the IPSP—this allowed us to place the model in an "anesthetized" regime while retaining the topological structure of the model.

bias, the up-regulation of $GABA_A$ receptors includes a targeting of the reticular nucleus of the thalamus, prolonging inhibitory post-synaptic potentials (Figure 1G), which in turn modulates its inhibition of both the core and matrix subpopulations. Thus, under IPSP prolongation, thalamocortical projections are weakened, in line with empirical observations.[47]

To test whether the model recapitulates systems-level empirical signatures of the anesthetized brain, we calculated a series of measures on the cortical ("*e*" in the *nftSim* model) population firing rates and BOLD-transformed activity. LFPs recorded from the macaque lateral intraparietal (LIP) cortex and frontal-eye fields (FEFs) show a decrease in coherent alpha-band activity under propofol anesthesia.[16] A comparison of homologous cortical regions in our model following a sweep of the anesthetic scaling, ρ, revealed a similar decline in alpha-band coherence between the FEF and LIP areas for $\rho = 1.12$ (Figures 2B and S3). In addition, functional connectivity changes following propofol include increased network dimensionality, $(\Delta \text{exp var } 1 = -19\% \pm 0.1\%)$, but also a reduction in network integration (mean participation coefficient: $\Delta PC = -4 \pm 0.1 \times 10^{-3}$). Timeseries show a reduction in susceptibility (sensitivity to perturbation[48]: $\Delta\chi = -18\% \pm 1\%$) and synchronization variability ($\Delta\sigma_\theta = -24\% \pm 1\%$), which captures the diversity of synchronous and asynchronous dynamics and represents a proxy for metastable switching between integrated and segregated modes. Of note, a measure of a system's memory, namely the mean autocorrelation timescale ($\Delta\tau_{ACF} = -34\% \pm 1\%$), also reduces following propofol. The fact that many of these signatures have previously been shown

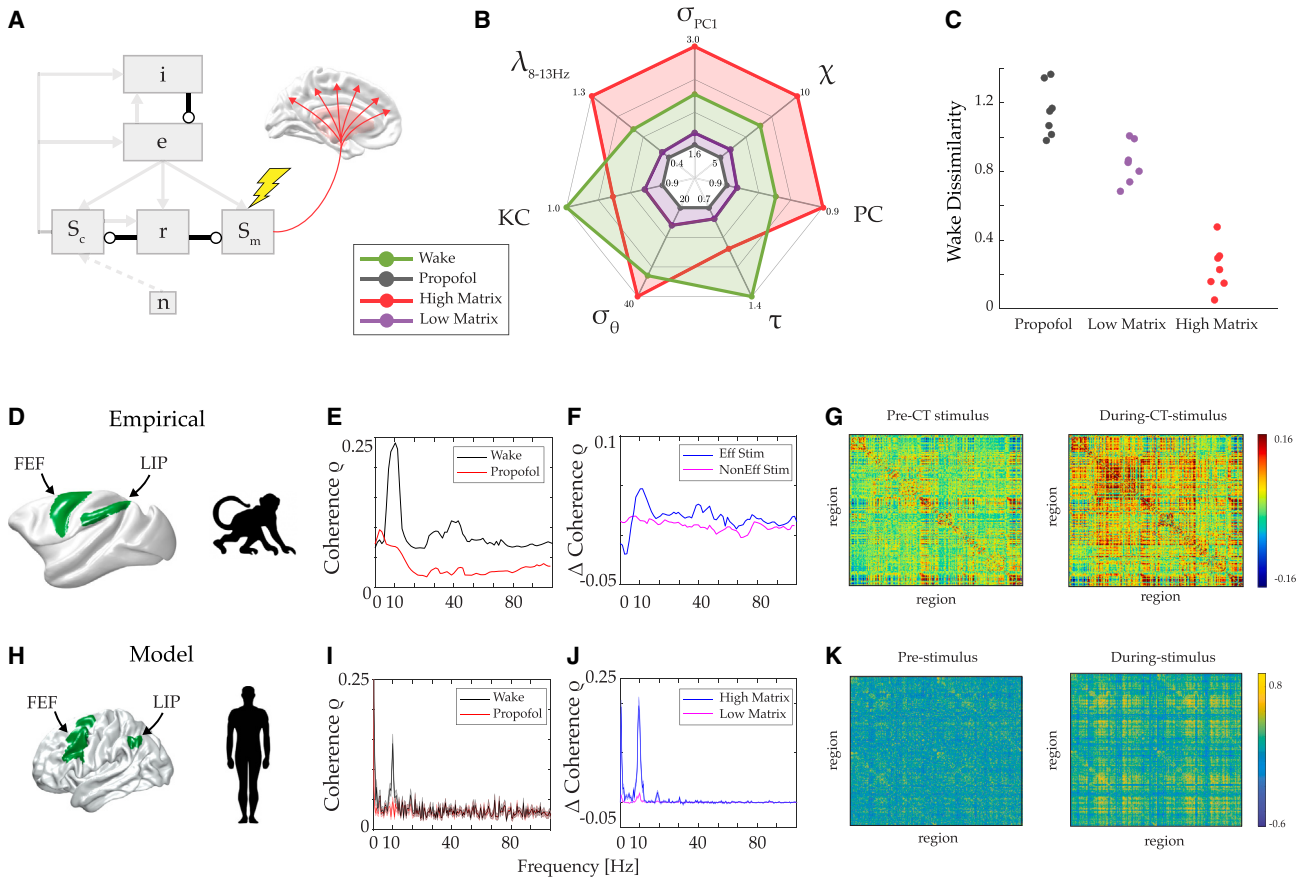

Figure 2. Propofol and corticocortical coherence

(A) Schema of targets for propofol effects and electrical stimulation of matrix thalamus. Emboldened connections show where the inhibitory post-synaptic potentials are prolonged under propofol—as shown in Figure 1G. Stimulation is applied exclusively to the matrix population.

(B) Measures of complex adaptive dynamics across wake (green), propofol (gray), and matrix stimulation (high: red, low: purple) states of the corticothalamic model: σ_{FC}, variance of functional connectivity; χ, susceptibility; PC, participation coefficient; τ, autocorrelation timescale; σ_θ, variance of phase synchrony; KC, Kolmogorov complexity; λ_{8-13Hz}, alpha-band (8–13 Hz) coherence; σ_{PC1}, explained variance of first principal component.

(C) Summation of percentage difference of each dynamics measure from wake values in propofol and matrix stimulation states. Each measure is jack-knifed to show effects on wake dissimilarity.

(D) Empirical macaque observations.

(E) Empirical coherence of monkey FEF and LIP cortical regions in wake and propofol anesthesia.

(F) Change in empirical coherence of monkey FEF and LIP under propofol anesthesia following central thalamic stimulation. Effective stimulation resulted in induced arousal in the monkey.

(E) and (F) are adapted from Redinbaugh et al.[16] and (G) is adapted from Tasserie et al.[17]

(G) Empirical functional connectivity of BOLD activity from a macaque monkey before and during stimulation of the central thalamus.

(H) Model human observations.

(I) Model coherence of FEF and LIP cortical activity in wake and propofol parameters.

(J) Change in coherence of FEF and LIP cortical activity for propofol vs. stimulation of high- and low-matrix regions.

(K) Functional connectivity of BOLD-transformed simulation cortical firing rates following high-matrix stimulation.

to change under anesthesia[49–53] provides a robust empirical validation of our neural mass model and thus allows us to test the hypothesis that simulation of the matrix thalamus can recover features of the awake brain (Figure 2A).

Electrophysiological recordings have shown a broad anteriorization of alpha-band activity (8–13 Hz) following propofol anesthesia,[54] and we find a similar topological pattern between wake and propofol model outputs (Figure S5). As this is an emergent property of the model, it suggests that the anteriorization of alpha activity emerges from the interaction between the thalamocortical gradient of core/matrix and cortical connectivity. In this way, our model predicts features not implicitly modeled.

The systems-level impact of matrix thalamic stimulation

We next characterized the impact of thalamic stimulation on corticocortical dynamics. Recent studies have shown that thalamic projections innervate both apical and basal dendrites of the L5 pyramidal tract (PT) neurons,[13,40] which, when driven together, allow calcium "spikes" to propagate to the soma and cause

high-frequency burst firing.[55] Furthermore, independent studies in anesthetized macaque found that central thalamic stimulation induced arousal-like behavioral states but at different stimulation frequencies (albeit using different types of stimulating electrodes and targeting different nuclei within the central thalamus).[16–18] Recent studies[56,57] have shown that the timescales of synaptodendritic and somatic dynamics (which impose a low-pass filter onto afferent signals) allow approximation of stimulus evoked responses by a constant perturbation that scales with stimulus frequency and amplitude (Figures S4A–S4C). We leveraged this to study the effects of stimulation applied to a target node of the matrix thalamus (Figure 2A), with exponentially decreasing amplitude as a function of geodesic distance for all other nodes. Thalamic regions are comprised of differential blends of core and matrix populations. To discern the effect of this on cortical dynamics, two separate simulations were run: the first targeted stimulation to a node with the highest proportion of matrix-to-core populations ("high matrix"; χ_H); the second targeted matrix stimulation to a node with the lowest proportion of matrix-to-core nuclei ("low matrix"; χ_L). Comparing these two thalamocortical extremes gives insight into their differential effect on cortico-cortical information processing.

A sweep of the stimulation amplitude and spatial decay rate parameters recapitulates the decrease in coherent alpha-band activity under propofol anesthesia observed empirically in macaque LFPs[16] and demonstrates that this model (Figure 2B) is robust across a range of parameter combinations (Figures S4E and S4F). For sufficiently large stimulation (large amplitude, spatial extent, or both), the model's dynamics cross a bifurcation and transition to a high-firing, seizure-like state.[24,30] This is consistent with empirical studies showing limbic seizure attenuation following inhibition of medial thalamus in rats,[58] suggesting that hyper-excitation of the medial thalamus plays an important role in generating epileptic states. For the following sections, we utilize a particular set of stimulus parameters (amplitude: 21 mV, decay rate: 6), although our findings are qualitatively consistent for all parameter values below the bifurcation boundary.

Simulation applied to χ_H areas facilitates a recovery of cortical firing rates to pre-propofol levels, with χ_H (but not χ_L) stimulation showing near full recovery (wake: $3.25 \pm 0.03\ s^{-1}$; χ_H stimulation: $2.98 \pm 0.11\ s^{-1}$; χ_L stimulation: $2.40 \pm 0.02\ s^{-1}$). In addition to recovering empirically observed alpha-band coherence,[16,17] χ_H stimulation yields a comparable recovery of low-dimensional functional connectivity (Δexpvar 1 = 32% ± 1%). Timeseries measures, including susceptibility ($\Delta\chi$ = 30% ± 1%), synchronization variability ($\Delta\sigma_\theta$ = 32% ± 1%), and mean autocorrelation timescales ($\Delta\tau_{ACF}$ = 20% ± 1%), likewise mirror recovery from their anesthesia suppression. To enumerate this effect, the similarity of propofol, χ_L, and χ_H stimulation states relative to wake were quantified by calculating the sum of normalized percentage differences (as shown in Figure 2C). This demonstrates that χ_H (but not χ_L) stimulation induces a change in complex adaptive dynamics that normalizes the brain to a state similar to wake.

Multi-electrode electrical stimulation of the central-lateral (CL) thalamus is found to promote conscious-like arousal,[16,59–62] and this effect was found to be markedly reduced with stimulation targets outside CL—in particular, the centromedian (CM) thalamus. To determine whether the stimulation site in the thalamus was consistent with empirical results, we inverted the thalamocortical gradient to make an estimate of which thalamic nuclei were stimulated in our model. Upon mapping stimulation targets in our model to a common thalamic atlas,[63] we find that high matrix strongly corresponds to stimulation of the CL thalamus (Figure S7A) and, conversely, low matrix to CM stimulation (Figure S7B). Thus, our model results are consistent with these empirical findings and provide further evidence for the role of matrix thalamus in supporting arousal states.

The role of the thalamus in cortical information processing

Next, we used three separate quantitative approaches to determine the role of the thalamus in shaping the response properties of the cortex in waking and under propofol anesthesia. Firstly, a 10 ms excitatory pulse was applied to the excitatory cortical population of two target areas in independent simulations (κ_H and κ_L) and then baseline normalized—note that these stimulations occurred on the cortical "*e*" populations and not the thalamic "*Sc/Sm*" populations (Figure 1B). We observed clear cortical evoked responses for both cortical targets, $\Delta Q_e \approx 5$ Hz (Figure 3A). Comparing these peak evoked responses across the cortex in both the wake and propofol conditions following cortical stimulation of the highest matrix region (κ_H; Figures 1D and 3D) revealed that the local response in the anesthetic state was similar to the awake, but the broader network response was an order of magnitude smaller in the anesthetic than in the awake state (Figure 3B). Furthermore, the normalized timeseries shows that rebound ripples—recurring waves of activity induced by the initial perturbation—are short lived under propofol relative to wake (Figure 3C), reflecting a reduced memory timescale. These patterns suggest that thalamocortical dynamics may at least partially underpin observed spatiotemporal traveling waves in resting-state cortical dynamics in humans.[64–66]

The differences in the consequences of stimulating cortical areas with either low- or high-matrix thalamic inputs (e.g., κ_H vs. κ_L) are evident from tracking the time-delayed activity pattern as it spreads across the cerebral cortex (Figure 3D). Notably, a serial activation pattern is observed for both targets (Figure 3D), indicative of a traveling wave emanating from the stimulus target site (Figure 3E). However, cortical responses to stimulation of κ_H are more strongly synchronized with a broad co-activation pattern (Figure 3D, left). This suggests that cortical regions that are tightly coupled to the matrix cells of the thalamus can signal broadly to other regions in parallel via the matrix thalamus and its influence on L5 PT neurons, thus providing a plausible neurobiological mechanism for modulating the formation and dissolution of the cortical coalitions required for flexible cognitive processing.[24]

To better quantify interregional information flow induced by the thalamus, we used two measures from information theory: information storage, which quantifies the amount of information in a system's past dynamics available to predict its future dynamics (Figure 4A), and information transfer/transfer entropy, which quantifies the amount of information in a system's past dynamics available to predict another system's future (Figure 4B).[67,64] Based on previous work,[65] we predicted that

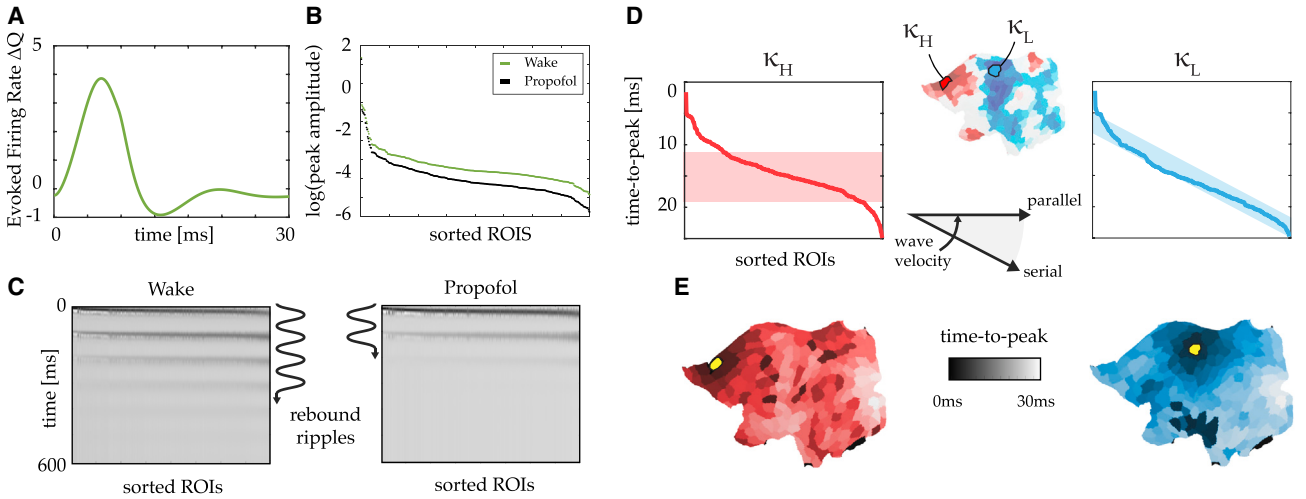

Figure 3. Perturbation dynamics

(A) Evoked response of target regions cortical firing rate, Q_e, following a 10 ms excitatory pulse applied to the cortical areas with the highest matrix thalamus projections.

(B) Peak evoked response for each cortical region following pulse stimulation sorted by amplitude. Wake results for the model are shown in green, and propofol results are shown in black.

(C) Timeseries of normalized evoked responses in the wake and propofol conditions. Regions of interest (ROIs) are sorted by amplitude.

(D) Single normalized evoked response for each cortical region following stimulation of a high- (κ_H) and low-matrix (κ_L) cortical region showing a propagating wave of evoked response with different wave velocities. The colored areas highlight significant wave velocity differences, with the high matrix showing more parallel activation of cortical areas (shaded red) than the more serial activation of regions seen following low-matrix stimulation (shaded blue).

(E) The spatial map of stimulus evoked response time to peak showing a propagating wave of evoked response that is not purely spatial. Stimulus targets are shown in yellow.

anesthesia should augment information storage, whereas stimulation of the matrix thalamus and waking dynamics should promote information transfer.[66] Consistent with these predictions, total information storage in our model was higher and more variable under propofol relative to awake ($\langle A_{wake}\rangle_i$ = 0.11 ± 0.002 [nats]; $\langle A_{prop}\rangle_i$ = 0.21 ± 0.003 [nats]; paired t: $p < 10^{-16}$; Figures 4Ai–4Aiv). χ_H stimulation diminishes these storage dynamics ($\langle A_{hi}\rangle_i$ = 0.16 ± 0.003 [nats]; paired t: $p < 10^{-16}$; Figure 4Aiii). In contrast, transfer entropy was highest and most variable in wake and χ_H stimulation conditions ($\langle T_{wake}\rangle_i$ = 0.17 ± 0.003 [nats]; $\langle T_{hi}\rangle_i$ = 0.21 ± 0.004 [nats]; Figures 4Biii and 4Biv) when compared with propofol and χ_L stimulation ($\langle T_{prop}\rangle_i$ = 0.078 ± 0.001 [bits]; paired t: $p < 10^{-16}$; $\langle T_{lo}\rangle_i$ = 0.09 ± 0.004 [nats]; paired t: $p < 10^{-16}$; Figures 4Bi–4Biii). Together, these results demonstrate that awake dynamics in our model constitute a mode of moderate information storage but high information transfer and that the matrix thalamus facilitates these corticocortical modes of information transfer.

Finally, we estimated the stability of systems-level neural dynamics following thalamic stimulation. To achieve this, we quantified the likelihood that the pattern of activity in the brain (i.e., the brain state) would change by a pre-specified amount (measured using the mean-squared displacement) in a specific window of time.[68] This captures the moment-to-moment stability of dynamics—difficult-to-reach brain states are associated with a high energy barrier, whereas unstable dynamics are associated with a low energy barrier (see STAR Methods). A comparison of simulated awake and propofol dynamics shows that anesthesia causes a steepening of the energy landscape, yielding slow and graded changes of dynamics (Figures 4A and 4B). That is, a brain state trajectory to an increasingly novel state is unlikely under propofol anesthesia when compared with the awake state. Interestingly, χ_H stimulation mimics the observed effects of noradrenergic arousal system[68] in that these cells act to flatten the energy landscape, making novel state trajectories more likely, restoring propofol states to the dynamic reconfigurations characteristic of the awake state.

DISCUSSION

Corticothalamic circuits support fundamental states of awareness and cognitive processes, but the mechanisms apportioned to different thalamic populations remain poorly understood. Here, we demonstrate that incorporating diffusely projecting, non-specific matrix nuclei of the thalamus into a whole-brain biophysical model facilitates integrated populations of pyramidal neurons in the cortex, supporting large-scale coherent signaling—a necessary condition for conscious awareness (Figure 1). Our biophysical model recapitulates several core empirical findings, including reduced cortical coherence following propofol anesthesia and its recovery following electrical stimulation of the matrix thalamus, as well as key features of complex adaptive systems (Figure 2). In addition, we demonstrate how the matrix thalamus instantiates a corticocortical communication hierarchy of parallel and serial processing modes (Figure 3) by facilitating flexible switching between dynamics modes of high information storage vs. high information transmission (Figure 4). This biophysically derived neural mass model thus advances our

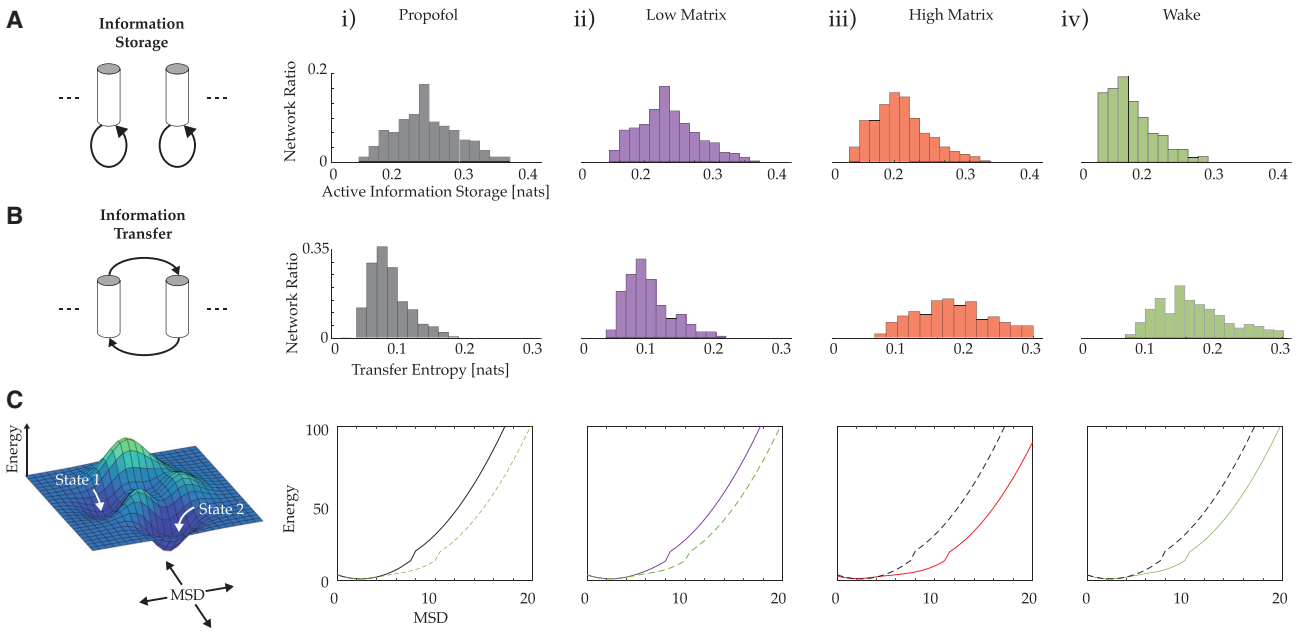

Figure 4. Information capacities and energy landscapes

(A) Active information storage of model firing rate timeseries.

(B) Transfer entropy of model firing rate timeseries.

(C) Mean-squared displacement of BOLD-transformed model firing rate states is calculated as a function of consecutive time points and the corresponding energy (logarithm of inverse state probability) of these states. Then, the average mean-squared displacement (MSD) vs. energy from a within a window of time (t = 0.12–0.155 s) is plotted. (i)–(iv) denote the four different states interrogated in our study.

understanding of the specific roles of thalamic subnuclei in supporting a broad repertoire of brain dynamics vital for awareness.

Electrophysiological recordings in humans[69] and macaque monkeys[16] have shown wide-spread changes in coherent cortical oscillatory dynamics following propofol anesthesia. Corticothalamic interactions have been argued to underpin these coherent dynamics[16,70,71]; however, the mechanisms through which this coordination occurs, and how the brain might exploit it while avoiding transition into a hyper-synchronized state (such as seizure), remains to be determined. In addition, distinct thalamocortical subclasses are known to display contrasting targeted (core) and diffuse (matrix) cortical projection profiles.[13,14,25] These subclasses have been shown to differentially augment key corticocortical interactions during perception[8,19,55,72] and are disrupted by anesthetics.[15] Deep brain electrical stimulation of the central thalamus in macaque monkeys has been shown to facilitate recovery of consciousness from propofol-induced loss of consciousness. Our model unifies our understanding of these independent empirical findings and provides evidence for the involvement of matrix thalamic nuclei in supporting large-scale coherent corticocortical communication important for consciousness and cognition.

Matrix-to-core proportions greatly vary across the thalamus, and the two extremes are present in the intralaminar thalamus, which is comprised of anterior and posterior cell groups.[73,74] In the anterior group, the CL nucleus contains nearly all calbindin cells and few parvalbumin cells (i.e., is high matrix, χ_H), whereas in the posterior group, the CM nucleus and the parafascicular nucleus contain nearly all parvalbumin cells and few calbindin cells (i.e., are low matrix, χ_L[75]). In our previous study,[16] we microstimulated via multiple closely spaced electrode contacts and localized contacts to different central thalamic nuclei. We measured the largest modulations of consciousness, and corresponding electrophysiological measures such as alpha coherence, when we stimulated the χ_H nucleus, CL.[16,59–61] As the location of stimulation sites moved further from the center of the CL nucleus (Figure S1 of Redinbaugh et al.[16]) to areas with lower matrix-to-core proportions, there was reduced modulation of consciousness, corresponding to reduced changes in electrophysiological measures. As a specific example, stimulating the low-matrix posterior intralaminar group corresponded to markedly reduced or little effect on consciousness (Figure 1 of Redinbaugh et al.[16]). These contrasting effects of stimulating high- and low-matrix sites *in vivo* match those generated here *in silico*.

In addition to supporting coherent cortical dynamics, our model predicts that the matrix thalamus facilitates several key dynamical features of a complex adaptive system. Notably, we find that the matrix thalamus promotes modes of high susceptibility as well as variability in synchronous activity—i.e., flexible shifts between segregated and integrated processing. In other words, the matrix thalamus provides a neurobiological platform for brain state complexity, as measured *in vivo*, with matrix stimulation modulating a heightened state of entropy and integrated information.[60,61] The mechanism through which the matrix thalamus facilitates this modulation is a process known as criticality[76,77]—for instance, a maximally susceptible system is one poised at a critical point (and vice versa).[78] To a first approximation, the diffuse projections of the matrix thalamus act analogous

to temperature in the Ising model and drive each corticothalamic region toward a locally defined critical point. This allows the system to support a wide range of distinct information processing benefits, including increased susceptibility, state diversity, prolonged timescales, and production of complex dynamic trajectories. In the present model, stimulating the matrix thalamus pushes the whole system toward criticality and can compensate for the reduction of connectivity resulting from anesthetic induced inhibition—which pushes it away from criticality—much like a temperature dial turning down under anesthetic and back up under thalamic stimulation. The brain undoubtedly has many mechanisms to provide this effect and likely can provide it in both more coarse as well as more targeted ways.[79] In particular, stimulation of other diffuse nuclei projecting to the cortex, such as the locus coeruleus, is predicted to provide a similar effect.

Information theory provides another formal perspective on the impact of the matrix thalamus in shaping cortical dynamics. Our results show that matrix projections to the cerebral cortex act to dissolve the local stable attractor dynamics supporting information storage in a manner that facilitates modes of high information transfer (Figure 4). These channels of information transfer follow the structural connectivity of our model and highlight how large-scale integration, via corticocortical structural connectivity, can be balanced with locally segregated information processing. Our results converge with previous modeling work, which revealed that, near a critical boundary of a neural system, changes in gain move the system into an integrated regime and act to increase transfer entropy[80] across a large-scale neural network while reducing active information storage.[65] Together, our results demonstrate how the diffusely projecting matrix thalamus may promote the formation (and dissolution) of unique ensembles of excitatory cortical populations to share information in such a way that catalyzes the formation of novel global brain states.

The corticothalamic system connects strongly with the neuromodulatory system,[21] which is strongly implicated in the neurobiology of arousal.[81] The impact of neuromodulatory neurotransmitters on the thalamus is well defined—acting via G protein-coupled second-messenger systems,[21] neurochemicals such as noradrenaline and acetylcholine cause a confirmational change in thalamic cells that closes a T-type calcium channel, thus allowing thalamic cells to spike in a tonic-firing mode characteristic of the awake brain. Similar effects are known to occur in the cerebral cortex[21,82,83] and highlight a key feature of the ascending neuromodulatory system—the widespread projections of the system implement a globally impactful signal that can be incorporated distinctly in target regions, depending on the presence (or absence) of specific neuromodulatory receptors.[53] We expect that the delineation of the precise interactions between the neuromodulatory system and the matrix thalamocortical mechanisms described in this article will accelerate our understanding of the manner in which the brain implements the processes that form the basis of a wide array of functional states. For instance, the diffuse projections of the matrix thalamus are still less diffuse than those of the locus coeruleus,[84] suggesting that the thalamus may provide a local augmentation of the systems-level topological effects mediated by the arousal system. In light of the rest of our findings, this feature may have important implications for supporting a diversity of active neural coalitions in parallel. Our model omits these interactions, and this presents an important avenue for future model extensions.

In previous work,[24] we showed that diffuse projections, be they from non-specific/matrix thalamocortical neurons or indeed noradrenergic subcorticocortical projections from the locus coeruleus, could promote quasi-critical states, forming a key component of consciousness and adaptive cognition. The present work applies this approach specifically to the matrix thalamus and its impact on the cerebral cortex and, in doing so, demonstrates how this principle can explain an empirical observation—namely that stimulation of specific thalamic regions is sufficient to recover consciousness under anesthetic. The effect of matrix thalamic stimulation on the whole corticothalamic system necessarily depends on state of the system when stimulation is applied. If the system was more inhibition dominant, stimulation may have the opposite effect. Crucially, this parameter regime would no longer reproduce key features used for empirical comparison, i.e., EEG and fMRI. That is why fitting the model before applying stimulation is crucial to ensuring that appropriate conclusions can be drawn from the stimulation's effect.

Limitations of the study

While the inclusion of different modeling elements is flexible, it is important to note that these model parameters are highly non-arbitrary in that they are based on decades of previous work that has been both theoretically and empirically verified across a range of experiments.[29,85] The primary benefit of our approach is that any emergent dynamics of our model are directly relatable to specific features of the neurobiological elements used to populate the model architecture. That is, the features of our model do not represent the only means by which similar emergent properties can be instantiated—rather, they represent a putative neurobiological mechanism through which the properties we measure from the system as a whole can be realistically explained. This is precisely why the fits to data, while far from perfect, represent such a crucial feature of this highly iterative process. That is, a model cannot rule out other mechanisms not considered—it can only provide candidate mechanisms that can (and should) be tested further experimentally. In the present study, we have demonstrated that diffuse connectivity from the matrix thalamus can explain the observation that thalamic stimulation can recover consciousness under anesthesia and, further, have provided understanding for the role of the thalamus in supporting corticocortical communication. Additional anatomical and neurochemical complexity not considered here will undoubtedly enrich this understanding and forms part of the essential interplay between theoretical and empirical approaches.

Another potential limitation of this work is the generalization of cortical firing rates to 3 Hz in order to balance excitation and inhibition in the model. While the heterogeneous core-matrix gradient breaks this homogeneity, defining regional specific firing rates as shown in Figure S9, unique cell types across the human brain demonstrate a diversity of firing rates not captured in the present model.[86,87] In addition, the granularity of cortical populations presented here—i.e., only two populations for the entire cerebral cortex—limits the translation of these

cell-specific firing rate distributions. The next iteration of large-scale models with a richer resolution of cortical populations will be able to tease apart these contributions and presents exciting avenues for future studies.

STAR★METHODS

Detailed methods are provided in the online version of this paper and include the following:

- KEY RESOURCES TABLE
- RESOURCE AVAILABILITY
  - Lead contact
  - Materials availability
  - Data and code availability
- EXPERIMENTAL MODEL AND STUDY PARTICIPANT DETAILS
  - Human neuroimaging dataset
- METHOD DETAILS
  - Corticothalamic model
  - Structural connectivity
  - Model balancing
  - Modeling propofol
  - Matrix stimulation
  - Human neuroimaging acquisition
  - Data pre-processing
- QUANTIFICATION AND STATISTICAL ANALYSIS
  - Complex adaptive dynamics measures
  - Information measures
  - Power spectral modes

SUPPLEMENTAL INFORMATION

Supplemental information can be found online at https://doi.org/10.1016/j.celrep.2023.112844.

ACKNOWLEDGMENTS

The authors would like to thank Matthew Larkum for stimulating discussions.

AUTHOR CONTRIBUTIONS

E.J.M. and J.M.S. conceived of the idea. E.J.M. designed and built the model and ran all analyses. B.R.M., M.J.R., J.L., M.B., and Y.B.S. provided critical methodological and conceptual input. E.J.M. and J.M.S. formulated the first draft of the manuscript. All authors provided critical feedback on the manuscript, including editing of the final manuscript.

DECLARATION OF INTERESTS

The authors declare no competing interests.

Received: December 1, 2022
Revised: April 25, 2023
Accepted: July 6, 2023

REFERENCES

1. Mashour, G.A., Roelfsema, P., Changeux, J.P., and Dehaene, S. (2020). Conscious Processing and the Global Neuronal Workspace Hypothesis. Neuron *105*, 776–798. https://doi.org/10.1016/j.neuron.2020.01.026.
2. Barttfeld, P., Uhrig, L., Sitt, J.D., Sigman, M., Jarraya, B., and Dehaene, S. (2015). Signature of consciousness in the dynamics of resting-state brain activity. Proc. Natl. Acad. Sci. USA *112*, 887–892. https://doi.org/10.1073/pnas.1418031112.
3. Hudetz, A.G., Liu, X., and Pillay, S. (2015). Dynamic repertoire of intrinsic brain states is reduced in propofol-induced unconsciousness. Brain Connect. *5*, 10–22. https://doi.org/10.1089/brain.2014.0230.
4. Huang, Z., Zhang, J., Wu, J., Liu, X., Xu, J., Zhang, J., Qin, P., Dai, R., Yang, Z., Mao, Y., et al. (2018). Disrupted neural variability during propofol-induced sedation and unconsciousness. Hum. Brain Mapp. *39*, 4533–4544. https://doi.org/10.1002/hbm.24304.
5. Casali, A.G., Gosseries, O., Rosanova, M., Boly, M., Sarasso, S., Casali, K.R., Casarotto, S., Bruno, M.-A., Laureys, S., Tononi, G., et al. A Theoretically Based Index of Consciousness Independent of Sensory Processing and Behavior.
6. Izhikevich, E.M., and Edelman, G.M. (2008). Large-scale Model of Mammalian Thalamocortical Systems.
7. Shine, J.M. (2021). The thalamus integrates the macrosystems of the brain to facilitate complex, adaptive brain network dynamics. Prog. Neurobiol. *199*, 101951. https://doi.org/10.1016/j.pneurobio.2020.101951.
8. Aru, J., Suzuki, M., Rutiku, R., Larkum, M.E., and Bachmann, T. (2019). Coupling the State and Contents of Consciousness. Front. Syst. Neurosci. *13*, 43. https://doi.org/10.3389/fnsys.2019.00043.
9. Llinäs, R.L., Ribary, U., Contreras, D., and Pedroarena, C. (1998). The Neuronal Basis for Consciousness.
10. Destexhe, A., and Sejnowski, T. (2001). Thalamocortical Assemblies: How Ion Channels, Single Neurons and Large-Scale Networks Organize Sleep Oscillations (Oxford University Press).
11. Contreras, D., Destexhe, A., Sejnowski, T.J., and Steriade, M. (1996). Control of Spatiotemporal Coherence of a Thalamic Oscillation by Corticothalamic Feedback Cort Icot Halamic Feedback Cont Rols Sleep Spindle Durat Ion in Vivo.
12. Destexhe, A., and Sejnowski, T.J. (2003). Interactions between Membrane Conductances Underlying Thalamocortical Slow-Wave Oscillations. https://doi.org/10.1152/physrev.00012.2003.-Neurons.
13. Clascá, F., Porrero, C., Galazo, M.J., Rubio-Garrido, P., and Evangelio, M. (2016). Anatomy and Development of Multispecific Thalamocortical Axons. Axons and Brain Architecture, 69–92. https://doi.org/10.1016/b978-0-12-801393-9.00004-9.
14. Jones, E.G. (2001). The thalamic matrix and thalamocortical synchrony. Trends Neurosci. *24*, 595–601. https://doi.org/10.1016/S0166-2236(00)01922-6.
15. Suzuki, M., and Larkum, M.E. (2020). General Anesthesia Decouples Cortical Pyramidal Neurons. Cell *180*, 666–676.e13. https://doi.org/10.1016/j.cell.2020.01.024.
16. Redinbaugh, M.J., Phillips, J.M., Kambi, N.A., Mohanta, S., Andryk, S., Dooley, G.L., Afrasiabi, M., Raz, A., and Saalmann, Y.B. (2020). Thalamus Modulates Consciousness via Layer-Specific Control of Cortex. Neuron *106*, 66–75.e12. https://doi.org/10.1016/j.neuron.2020.01.005.
17. Tasserie, J., Uhrig, L., Sitt, J.D., Manasova, D., Dupont, M., Dehaene, S., and Jarraya, B. (2022). Deep brain stimulation of the thalamus restores signatures of consciousness in a nonhuman primate model.
18. Bastos, A.M., Donoghue, J.A., Brincat, S.L., Mahnke, M., Yanar, J., Correa, J., Waite, A.S., Lundqvist, M., Roy, J., Brown, E.N., and Miller, E.K. (2021). Neural effects of propofol-induced unconsciousness and its reversal using thalamic stimulation. Elife *10*, e60824. https://doi.org/10.7554/ELIFE.60824.
19. Aru, J., Suzuki, M., and Larkum, M.E. (2020). Cellular Mechanisms of Conscious Processing. Trends Cogn. Sci. *24*, 814–825. https://doi.org/10.1016/j.tics.2020.07.006.
20. Honjoh, S., Sasai, S., Schiereck, S.S., Nagai, H., Tononi, G., and Cirelli, C. (2018). Regulation of cortical activity and arousal by the matrix cells

of the ventromedial thalamic nucleus. Nat. Commun. *9*, 2100. https://doi.org/10.1038/s41467-018-04497-x.

21. Shine, J.M., Müller, E.J., Munn, B., Cabral, J., Moran, R.J., and Breakspear, M. (2021). Computational models link cellular mechanisms of neuromodulation to large-scale neural dynamics. Nat. Neurosci. *24*, 765–776. https://doi.org/10.1038/s41593-021-00824-6.
22. Breakspear, M. (2017). Dynamic models of large-scale brain activity. Nat. Neurosci. *20*, 340–352. https://doi.org/10.1038/nn.4497.
23. Kringelbach, M.L., and Deco, G. (2020). Brain States and Transitions: Insights from Computational Neuroscience. Cell Rep. *32*, 108128. https://doi.org/10.1016/j.celrep.2020.108128.
24. Müller, E.J., Munn, B., and Shine, J.M. (2020). Diffuse neural coupling mediates complex network dynamics through the formation of quasi-critical brain states. Nat. Commun. https://doi.org/10.1101/2020.06.09.141416.
25. Müller, E.J., Munn, B., Hearne, L.J., Smith, J.B., Fulcher, B., Arnatkevičiūtė, A., Lurie, D.J., Cocchi, L., and Shine, J.M. (2020). Core and matrix thalamic sub-populations relate to spatio-temporal cortical connectivity gradients. Neuroimage *222*, 117224. https://doi.org/10.1016/j.neuroimage.2020.117224.
26. Noroozbabaee, L., Steyn-Ross, D.A., Steyn-Ross, M.L., and Sleigh, J.W. (2021). Analysis of the Hindriks and van Putten model for propofol anesthesia: Limitations and extensions. Neuroimage *227*, 117633. https://doi.org/10.1016/j.neuroimage.2020.117633.
27. Schaefer, A., Kong, R., Gordon, E.M., Laumann, T.O., Zuo, X.-N., Holmes, A.J., Eickhoff, S.B., and Yeo, B.T.T. (2018). Local-Global Parcellation of the Human Cerebral Cortex from Intrinsic Functional Connectivity MRI. Cereb. Cortex *28*, 3095–3114. https://doi.org/10.1093/cercor/bhx179.
28. Sanz-Leon, P., Robinson, P.A., Knock, S.A., Drysdale, P.M., Abeysuriya, R.G., Fung, F.K., Rennie, C.J., and Zhao, X. (2018). NFTsim: Theory and Simulation of Multiscale Neural Field Dynamics. https://doi.org/10.1371/journal.pcbi.1006387.
29. Robinson, P.A., Rennie, C.J., Wright, J.J., and Bourke, P.D. (1998). Steady states and global dynamics of electrical activity in the cerebral cortex. Phys. Rev. E *58*, 3557–3571. https://doi.org/10.1103/PhysRevE.58.3557.
30. Robinson, P.A., Rennie, C.J., and Rowe, D.L. (2002). Dynamics of large-scale brain activity in normal arousal states and epileptic seizures. Phys. Rev. E Stat. Nonlin. Soft Matter Phys. *65*, 041924. https://doi.org/10.1103/PhysRevE.65.041924.
31. Jirsa, V.K., and Haken, H. (1996). Field theory of electromagnetic brain activity. Phys. Rev. Lett. *77*, 960–963. https://doi.org/10.1103/PhysRevLett.77.960.
32. Deco, G., and Jirsa, V.K. (2012). Ongoing Cortical Activity at Rest: Criticality, Multistability, and Ghost Attractors. J. Neurosci. *32*, 3366–3375. https://doi.org/10.1523/jneurosci.2523-11.2012.
33. Abeysuriya, R.G., Rennie, C.J., and Robinson, P.A. (2015). Physiologically based arousal state estimation and dynamics. J. Neurosci. Methods *253*, 55–69. https://doi.org/10.1016/j.jneumeth.2015.06.002.
34. Buzsáki, G., Anastassiou, C.A., and Koch, C. (2012). The origin of extracellular fields and currents-EEG, ECoG, LFP and spikes. Nat. Rev. Neurosci. *13*, 407–420. https://doi.org/10.1038/nrn3241.
35. Horvát, S., Gămănuț, R., Ercsey-Ravasz, M., Magrou, L., Gămănuț, B., van Essen, D.C., Burkhalter, A., Knoblauch, K., Toroczkai, Z., and Kennedy, H. (2016). Spatial Embedding and Wiring Cost Constrain the Functional Layout of the Cortical Network of Rodents and Primates. PLoS Biol. *14*, e1002512. https://doi.org/10.1371/journal.pbio.1002512.
36. Ercsey-Ravasz, M., Markov, N.T., Lamy, C., VanEssen, D.C., Knoblauch, K., Toroczkai, Z., and Kennedy, H. (2013). A Predictive Network Model of Cerebral Cortical Connectivity Based on a Distance Rule. Neuron *80*, 184–197. https://doi.org/10.1016/j.neuron.2013.07.036.
37. Henderson, J.A., and Robinson, P.A. (2014). Relations between the geometry of cortical gyrification and white-matter network architecture. Brain Connect. *4*, 112–130. https://doi.org/10.1089/brain.2013.0183.
38. Henderson, J.A., and Robinson, P.A. (2013). Using geometry to uncover relationships between isotropy, homogeneity, and modularity in cortical connectivity. Brain Connect. *3*, 423–437. https://doi.org/10.1089/brain.2013.0151.
39. Royer, J., Rodríguez-Cruces, R., Tavakol, S., Larivière, S., Herholz, P., Li, Q., Vos de Wael, R., Paquola, C., Benkarim, O., Park, B.Y., et al. (2022). An Open MRI Dataset For Multiscale Neuroscience. Sci. Data *9*, 569. https://doi.org/10.1038/s41597-022-01682-y.
40. Shepherd, G.M.G., and Yamawaki, N. (2021). Untangling the cortico-thalamo-cortical loop: cellular pieces of a knotty circuit puzzle. Nat. Rev. Neurosci. *22*, 389–406. https://doi.org/10.1038/s41583-021-00459-3.
41. Messé, A., Rudrauf, D., Giron, A., and Marrelec, G. (2015). Predicting functional connectivity from structural connectivity via computational models using MRI: An extensive comparison study. Neuroimage *111*, 65–75. https://doi.org/10.1016/j.neuroimage.2015.02.001.
42. Wischnewski, K.J., Eickhoff, S.B., Jirsa, V.K., and Popovych, O.v. (2022). Towards an efficient validation of dynamical whole-brain models. Sci. Rep. *12*, 4331. https://doi.org/10.1038/s41598-022-07860-7.
43. Iascone, D.M., Li, Y., Sümbül, U., Doron, M., Chen, H., Andreu, V., Goudy, F., Blockus, H., Abbott, L.F., Segev, I., et al. (2020). Whole-Neuron Synaptic Mapping Reveals Spatially Precise Excitatory/Inhibitory Balance Limiting Dendritic and Somatic Spiking. Neuron *106*, 566–578.e8. https://doi.org/10.1016/j.neuron.2020.02.015.
44. Deco, G., Ponce-Alvarez, A., Hagmann, P., Romani, G.L., Mantini, D., and Corbetta, M. (2014). How local excitation-inhibition ratio impacts the whole brain dynamics. J. Neurosci. *34*, 7886–7898. https://doi.org/10.1523/JNEUROSCI.5068-13.2014.
45. De Kock, C.P.J., and Sakmann, B. (2008). High frequency action potential bursts (≥ 100 Hz) in L2/3 and L5B thick tufted neurons in anaesthetized and awake rat primary somatosensory cortex. J. Physiol. *586*, 3353–3364. https://doi.org/10.1113/jphysiol.2008.155580.
46. Hearne, L.J., Cocchi, L., Zalesky, A., and Mattingley, J.B. (2017). Reconfiguration of brain network architectures between resting-state and complexity-dependent cognitive reasoning. J. Neurosci. *37*, 8399–8411. https://doi.org/10.1523/JNEUROSCI.0485-17.2017.
47. Franks, N.P. (2008). General anesthesia: From molecular targets to neuronal pathways of sleep and arousal. Nat. Rev. Neurosci. *9*, 370–386. https://doi.org/10.1038/nrn2372.
48. Yu, S., Yang, H., Shriki, O., and Plenz, D. (2013). Universal organization of resting brain activity at the thermodynamic critical point. Front. Syst. Neurosci. *7*, 42. https://doi.org/10.3389/fnsys.2013.00042.
49. Deco, G., Kringelbach, M.L., Jirsa, V.K., and Ritter, P. (2017). The dynamics of resting fluctuations in the brain: Metastability and its dynamical cortical core. Sci. Rep. *7*, 3095. https://doi.org/10.1038/s41598-017-03073-5.
50. Hudetz, A.G., Liu, X., Pillay, S., Boly, M., and Tononi, G. (2016). Propofol anesthesia reduces Lempel-Ziv complexity of spontaneous brain activity in rats. Neurosci. Lett. *628*, 132–135. https://doi.org/10.1016/j.neulet.2016.06.017.
51. Sanz Perl, Y., Pallavicini, C., Pérez Ipiña, I., Demertzi, A., Bonhomme, V., Martial, C., Panda, R., Annen, J., Ibañez, A., Kringelbach, M., et al. (2021). Perturbations in dynamical models of wholebrain activity dissociate between the level and stability of consciousness. PLoS Comput. Biol. *17*, e1009139. https://doi.org/10.1371/journal.pcbi.1009139.
52. Balaguer-Ballester, E., Moreno-Bote, R., Deco, G., and Durstewitz, D. (2017). Editorial: Metastable Dynamics of Neural Ensembles. Front. Syst. Neurosci. *11*, 99. https://doi.org/10.3389/fnsys.2017.00099.
53. Shine, J.M., Breakspear, M., Bell, P.T., Ehgoetz Martens, K.A., Shine, R., Koyejo, O., Sporns, O., and Poldrack, R.A. (2019). Human cognition involves the dynamic integration of neural activity and neuromodulatory

systems. Nat. Neurosci. *22*, 289–296. https://doi.org/10.1038/s41593-018-0312-0.

54. Purdon, P.L., Pierce, E.T., Mukamel, E.A., Prerau, M.J., Walsh, J.L., Wong, K.F.K., Salazar-Gomez, A.F., Harrell, P.G., Sampson, A.L., Cimenser, A., et al. (2013). Electroencephalogram signatures of loss and recovery of consciousness from propofol. Proc. Natl. Acad. Sci. USA *110*, E1142, E1151. https://doi.org/10.1073/pnas.1221180110.
55. Guest, J.M., Bast, A., Narayanan, R.T., and Oberlaender, M. (2021). Thalamus Gates Active Dendritic Computations in Cortex during Sensory Processing, pp. 1–14.
56. Müller, E.J., and Robinson, P.A. (2018). Quantitative theory of deep brain stimulation of the subthalamic nucleus for the suppression of pathological rhythms in Parkinson's disease. PLoS Comput. Biol. *14*, 1–20. https://doi.org/10.1371/journal.pcbi.1006217.
57. Müller, E.J., and Robinson, P.A. (2018). Suppression of Parkinsonian Beta Oscillations by Deep Brain Stimulation: Determination of Effective Protocols. Front. Comput. Neurosci. *12*, 98. https://doi.org/10.3389/fncom.2018.00098.
58. Wicker, E., and Forcelli, P.A. (2021). Optogenetic activation of the reticular nucleus of the thalamus attenuates limbic seizures via inhibition of the midline thalamus. Epilepsia *62*, 2283–2296. https://doi.org/10.1111/epi.17016.
59. Redinbaugh, M.J., Afrasiabi, M., Phillips, J.M., Kambi, N.A., Mohanta, S., and S, Y.B. (2021). Thalamic Deep Brain Stimulation as a Paradigm to Reduce Consciousness: Implications for Cortico-Striatal Dynamics, Absence Epilepsy and Consciousness Studies, *6*.
60. Redinbaugh, M.J., Afrasiabi, M., Phillips, J.M., Kambi, N.A., Mohanta, S., Raz, A., and Saalmann, Y.B. (2022). Thalamic deep brain stimulation paradigm to reduce consciousness: Cortico-striatal dynamics implicated in mechanisms of consciousness. PLoS Comput. Biol. *18*, e1010294. https://doi.org/10.1371/journal.pcbi.1010294.
61. Afrasiabi, M., Redinbaugh, M.J., Phillips, J.M., Kambi, N.A., Mohanta, S., Raz, A., Haun, A.M., and Saalmann, Y.B. (2021). Consciousness depends on integration between parietal cortex, striatum, and thalamus. Cell Syst. *12*, 363–373.e11. https://doi.org/10.1016/j.cels.2021.02.003.
62. Redinbaugh, M.J., Phillips, J.M., Kambi, N.A., Mohanta, S., Andryk, S., Dooley, G.L., Afrasiabi, M., Raz, A., and Saalmann, Y. (2019). Thalamus Modulates Consciousness Via Layer-Specific Control of Cortex. SSRN Journal, 1–10. https://doi.org/10.2139/ssrn.3493781.
63. Morel, A., Magnin, M., and Jeanmonod, D. (1997). Multiarchitectonic and Stereotactic Atlas of the Human Thalamus (Wiley-Liss, Inc).
64. Lizier, J.T., Prokopenko, M., and Zomaya, A.Y. (2012). Local measures of information storage in complex distributed computation. Inf. Sci. *208*, 39–54. https://doi.org/10.1016/j.ins.2012.04.016.
65. Li, M., Han, Y., Aburn, M.J., Breakspear, M., Poldrack, R.A., Shine, J.M., and Lizier, J.T. (2019). Transitions in information processing dynamics at the whole-brain network level are driven by alterations in neural gain. PLoS Comput. Biol. *15*, e1006957. https://doi.org/10.1371/journal.pcbi.1006957.
66. Liang, Z., Cheng, L., Shao, S., Jin, X., Yu, T., Sleigh, J.W., and Li, X. (2020). Information integration and mesoscopic cortical connectivity during propofol anesthesia. Anesthesiology *132*, 504–524. https://doi.org/10.1097/ALN.0000000000003015.
67. Lizier, J.T. (2014). JIDT: an information-theoretic toolkit for studying the dynamics of complex systems. Front. Robot. AI *1*. https://doi.org/10.3389/frobt.2014.00011.
68. Munn, B.R., Müller, E.J., Wainstein, G., and Shine, J.M. (2021). The ascending arousal system shapes neural dynamics to mediate awareness of cognitive states. Nat. Commun. *12*, 1–9. https://doi.org/10.1038/s41467-021-26268-x.
69. Purdon, P.L., Pierce, E.T., Mukamel, E.A., Prerau, M.J., Walsh, J.L., Wong, K.F.K., Salazar-Gomez, A.F., Harrell, P.G., Sampson, A.L., Cimenser, A., et al. (2013). Electroencephalogram signatures of loss and recovery of consciousness from propofol. Proc. Natl. Acad. Sci. USA *110*, E1142, E1151. https://doi.org/10.1073/pnas.1221180110.
70. Destexhe, A., Contreras, D., and Steriade, M. (1999). Cortically-induced coherence of a thalamic-generated oscillation. Neuroscience *92*, 427–443. https://doi.org/10.1016/S0306-4522(99)00024-X.
71. Vijayan, S., Ching, S., Purdon, P.L., Brown, E.N., and Kopell, N.J. (2013). Thalamocortical mechanisms for the anteriorization of alpha rhythms during propofol-induced unconsciousness. J. Neurosci. *33*, 11070–11075. https://doi.org/10.1523/JNEUROSCI.5670-12.2013.
72. Takahashi, N., Oertner, T.G., Hegemann, P., and Larkum, M.E. (2016). Active cortical dendrites modulate perception*354*, pp. 1587–1590. https://doi.org/10.1126/science.aah6066.
73. Jones, E.G., and Hendry, S.H.C. (1989). Differential Calcium Binding Protein Immunoreactivity Distinguishes Classes of Relay Neurons in Monkey Thalamic Nuclei. Eur. J. Neurosci. *1*, 222–246. https://doi.org/10.1111/j.1460-9568.1989.tb00791.x.
74. Münkle, M.C., Waldvogel, H.J., and Faull, R.L.M. (1999). Calcium-binding protein immunoreactivity delineates the intralaminar nuclei of the thalamus in the human brain. Neuroscience *90*, 485–491.
75. Jones, E.G. (1998). Viewpoint: the core and matrix of thalamic organization. Neuroscience *85*, 331–345. https://doi.org/10.1016/S0306-4522(97)00581-2.
76. Cocchi, L., Gollo, L.L., Zalesky, A., and Breakspear, M. (2017). Criticality in the brain: A synthesis of neurobiology, models and cognition. Prog. Neurobiol. *158*, 132–152. https://doi.org/10.1016/j.pneurobio.2017.07.002.
77. Muñoz, M.A. (2018). Colloquium: Criticality and dynamical scaling in living systems. Rev. Mod. Phys. *90*, 031001. https://doi.org/10.1103/RevModPhys.90.031001.
78. Cipra, B.A. (1987). An Introduction to the Ising Model.
79. Shine, J.M. (2023). Neuromodulatory control of complex adaptive dynamics in the brain. Interface Focus *13*, 20220079. https://doi.org/10.1098/rsfs.2022.0079.
80. Wollstadt, P., Sellers, K.K., Rudelt, L., Priesemann, V., Hutt, A., Fröhlich, F., and Wibral, M. (2017). Breakdown of local information processing may underlie isoflurane anesthesia effects. PLoS Comput. Biol. *13*, e1005511. https://doi.org/10.1371/journal.pcbi.1005511.
81. Brown, E.N., Purdon, P.L., and van Dort, C.J. (2011). General anesthesia and altered states of arousal: A systems neuroscience analysis. Annu. Rev. Neurosci. *34*, 601–628. https://doi.org/10.1146/annurev-neuro-060909-153200.
82. Labarrera, C., Deitcher, Y., Dudai, A., Weiner, B., Kaduri Amichai, A., Zylbermann, N., and London, M. (2018). Adrenergic Modulation Regulates the Dendritic Excitability of Layer 5 Pyramidal Neurons In Vivo. Cell Rep. *23*, 1034–1044. https://doi.org/10.1016/j.celrep.2018.03.103.
83. Williams, S.R., and Fletcher, L.N. (2019). A Dendritic Substrate for the Cholinergic Control of Neocortical Output Neurons. Neuron *101*, 486–499.e4. https://doi.org/10.1016/j.neuron.2018.11.035.
84. Wainstein, G., Müller, E.J., Taylor, N., Munn, B., and Shine, J.M. (2022). The role of the locus coeruleus in shaping adaptive cortical melodies. Trends Cogn. Sci. *26*, 527–538. https://doi.org/10.1016/j.tics.2022.03.006.
85. Robinson, P.A., Rennie, C.J., Rowe, D.L., and O'Connor, C. (2004). Estimation of multiscale neurophysiologic parameters by electroencephalographic means. Hum. Brain Mapp. *23*, 53–72. https://doi.org/10.1002/hbm.20032.
86. Harris, K.D., and Shepherd, G.M.G. (2015). The neocortical circuit: Themes and variations. Nat. Neurosci. *18*, 170–181. https://doi.org/10.1038/nn.3917.
87. Clascá, F., Rubio-Garrido, P., and Jabaudon, D. (2012). Unveiling the diversity of thalamocortical neuron subtypes. Eur. J. Neurosci. *35*, 1524–1532. https://doi.org/10.1111/j.1460-9568.2012.08033.x.

88. Abeysuriya, R.G., and Robinson, P.A. (2016). Real-time automated EEG tracking of brain states using neural field theory. J. Neurosci. Methods *258*, 28–45. https://doi.org/10.1016/j.jneumeth.2015.09.026.

89. Robinson, P.A., Loxley, P.N., O'Connor, S.C., and Rennie, C.J. (2001). Modal analysis of corticothalamic dynamics, electroencephalographic spectra, and evoked potentials. Phys. Rev. E Stat. Nonlin. Soft Matter Phys. *63*, 041909–041913. https://doi.org/10.1103/PhysRevE.63.041909.

90. Robinson, P.A., Rennie, C.J., Wright, J.J., Bahramali, H., Gordon, E., and Rowe, D.L. (2001). Prediction of electrocnccphulographic spectra from neurophysiology. Phys. Rev. E Stat. Nonlin. Soft Matter Phys. *63*, 021903–02190318. https://doi.org/10.1103/PhysRevE.63.021903.

91. Fischl, B. (2012). Neuroimage *62*, 774–781. https://doi.org/10.1016/j.neuroimage.2012.01.021.

92. Hearne, L.J., Cocchi, L., Zalesky, A., and Mattingley, J.B. (2017). Reconfiguration of brain network architectures between resting-state and complexity-dependent cognitive reasoning. J. Neurosci. *37*, 8399–8411. https://doi.org/10.1523/JNEUROSCI.0485-17.2017.

93. Wright, J.J., and Liley, D.T.J. (1996). Dynamics of the brain at global and microscopic scales: Neural networks and the EEG. Behav. Brain Sci. *19*, 285–295. https://doi.org/10.1017/s0140525x00042679.

94. Braitenberg, V., and Schuz, A. (2013). Cortex: Statistics and Geometry of Neuronal Connectivity.

95. Unzai, T., Kuramoto, E., Kaneko, T., and Fujiyama, F. (2017). Quantitative Analyses of the Projection of Individual Neurons from the Midline Thalamic Nuclei to the Striosome and Matrix Compartments of the Rat Striatum. Cereb. Cortex *27*, 1164–1181. https://doi.org/10.1093/cercor/bhv295.

96. Lliná, R.R., Leznik, E., and Urbano, F.J. (2001). Temporal Binding via Cortical Coincidence Detection of Specific and Nonspecific Thalamocortical Inputs: A Voltage-dependent Dye-Imaging Study in Mouse Brain Slices.

97. Crabtree, J.W., and Isaac, J.T.R. (2002). New Intrathalamic Pathways Allowing Modality-Related and Cross-Modality Switching in the Dorsal Thalamus.

98. van der Werf, Y.D., Witter, M.P., and Groenewegen, H.J. (2002). T he intralaminar and midline nuclei of the thalamus. Anatomical and Functional Evidence for Participation in Processes of Arousal and Awareness.

99. Behzadi, Y., Restom, K., Liau, J., and Liu, T.T. (2007). A component based noise correction method (CompCor) for BOLD and perfusion based fMRI. Neuroimage *37*, 90–101. https://doi.org/10.1016/j.neuroimage.2007.04.042.

100. Erten, E., Lizier, J., Piraveenan, M., and Prokopenko, M. (2017). Criticality and information dynamics in epidemiological models. Entropy *19*, 194. https://doi.org/10.3390/e19050194.

101. Garland, J., James, R.G., and Bradley, E. (2016). Leveraging information storage to select forecast-optimal parameters for delay-coordinate reconstructions. Phys. Rev. E *93*, 022221. https://doi.org/10.1103/PhysRevE.93.022221.

STAR★METHODS

KEY RESOURCES TABLE

REAGENT or RESOURCE	SOURCE	IDENTIFIER
Deposited data		
Human neuroimaging regional correlations	This paper	Zenodo: https://doi.org/10.5281/zenodo.8072497
Software and algorithms		
MATLAB	The mathworks	www.mathworks.com
nftSim	Sanz-Leon et al.[27]	github.com/BrainDynamicsUSYD/nftsim
Model and data analysis source code	This paper	Zenodo: https://doi.org/10.5281/zenodo.8072497

RESOURCE AVAILABILITY

Lead contact

Further information and requests for resources should be directed to Eli Muller (eli.muller@sydney.edu.au).

Materials availability

This study did not generate unique reagents.

Data and code availability

- The data reported in this paper will be shared by the lead contact upon request.
- Any additional information required to reanalyze the data reported in this paper is available from the lead contact upon request.
- All original code has been deposited at https://github.com/elimuller/Corticothalamic_CM_model and is publicly available as of the date of publication. DOIs are listed in the key resources table.

EXPERIMENTAL MODEL AND STUDY PARTICIPANT DETAILS

Human neuroimaging dataset

Participants

Sixty-five healthy, right-handed adult participants (18–33 years) were recruited, of whom 60 were included in the final analysis (28 females). Participants provided informed written consent to participate in the study. The research was approved by The University of Queensland Human Research Ethics Committee. These data were originally described in.[46]

METHOD DETAILS

Corticothalamic model

The corticothalamic model consists of 400 coupled neural masses. We outline this architecture by first detailing the corticothalamic neural mass as follows. The corticothalamic neural mass model used in this work contains four distinct populations: an excitatory pyramidal cell, e, and an inhibitory interneuron, i, population in the cortex; and two excitatory nuclei, matrix, s_m; core, s_c, and inhibitory thalamic reticular nuclei, r, population in the thalamus (Figure 1C). The dynamical processes that occur within and between populations in a neural field model are defined as follows:

For each population, the mean soma potential results from incoming postsynaptic potentials (PSPs):

$$V_a(t) = \sum_b V_{ab}(t) \quad \text{(Equation 1)}$$

where $V_{ab}(t)$ is the result of a postsynaptic potential of type b onto a neuron of type a and $a,b \in \{e,i,r,s\}$. The postsynaptic potential response in the dendrite is given by

$$D_{ab}V_{ab}(t) = \nu_{ab}\varphi_{ab}(t - \tau_{ab}) \quad \text{(Equation 2)}$$

where the influence of incoming spikes to population a from population b is weighted by a connection strength parameter $\nu_{ab} = N_{ab}s_{ab}$, with the mean number of connections between the two populations N_{ab} and s_{ab} is the mean strength of response in neuron a to a single spike from neuron b. τ_{ab} is the average axonal delay for the transmission of signals, and φ_{ab} is the mean axonal pulse rate from b to a.

The operator D_{ab} describes the time evolution of V_{ab} in response to synaptic input,

$$D_{ab} = \frac{1}{\alpha\beta}\frac{d^2}{dt^2} + \left(\frac{1}{\alpha} + \frac{1}{\beta}\right)\frac{d}{dt} + 1 \quad \text{(Equation 3)}$$

where β and α are the overall rise and decay response rates to the synaptodendritic and soma dynamics.

The mean firing rate of a neural population $Q_a(t)$ can be approximately related to its mean membrane potential, $V_a(t)$, by,

$$Q_a(t) = S_a[V_a(t)] = \frac{Q_a^{max}}{1+\exp[-\{V_a(t) - \theta_a\}/\sigma']} \quad \text{(Equation 4)}$$

which define a sigmoidal mapping function S_a with a maximal firing rate Q_a^{max}, a mean firing threshold θ_a, and a standard deviation of this threshold $\sigma'\pi/\sqrt{3}$.

The mean axonal pulse rate is related to the mean firing rate by,

$$D_a(t)\varphi_a(t) = Q_a(t) \quad \text{(Equation 5)}$$

$$D_a(t) = \frac{1}{\gamma_a^2}\frac{\partial^2}{\partial t^2} + \frac{2}{\gamma_a}\frac{\partial}{\partial t} + 1 \quad \text{(Equation 6)}$$

here, $\gamma_a = v_a/r_a$ represents the damping rate, where v_a is the propagation velocity in axons, and r_a is the characteristic axonal length for the population.

A network of 400 corticothalamic neural masses were simulated using the neural field simulation software, *nftSim*.[28] The parameters for each neural mass were identically set to *"eyes-closed"* estimates given in Table 1,[28,30,33,85,88] which results in simulated activity with a 1/f spectrum and a peak in the alpha frequency band (8–13 Hz) in the absence of network coupling. These are example parameters representative of the "*eyes-closed*" state following Bayesian model fits to human EEG power spectra.[33] Many preceding studies[29,30,33,85,88–90] have shown the linear transfer function, which drives the linear spectral content of the corticothalamic model, is derived and shown to be low-dimensional, i.e., only a few loop gains in the system are needed to capture the key features of the power spectra. In this particular context, the eyes-closed state of human EEG has a 1/f slope and a spectral peak at in the 8-13Hz alpha frequency band, and this is explained by a weakly damped thalamocortical loop gain (ese). For the present study we have selected characteristic parameters for this power spectrum (Table 7 from[33]). Note that this spectrum describes modulations of firing rate around a fixed point, which are static for the network (see Figure S9). These spike rate modulations in neurons drive changes in the extracellular electric field which are then measured via EEG and LFP recordings.[34] In this way, we are able to compare our model outputs to empirical data through the power spectral density function.

Each simulation was run for a total of 64s with 7.5s of initial transients removed using an integration timestep of $\Delta t = 2^{-13}$ s. This minimizes contributions from the model's initial state and ensures the integration algorithm has stabilized before we begin analysing simulation outputs. Longer simulations produced qualitatively identical results, as did shorter simulations (see Figure S8) however, many of the analysis measures presented in this paper perform better with more data – i.e., correlation and coherence are noisier with less data. Thus, a balance between metric accuracy, resource allotment, and tractability for dataset manipulations was chosen. All outputs were down-sampled to 200Hz for tractability. All remaining data was used for subsequent analysis.

Structural connectivity

The structural connectivity used to define the model network consists of a combination of distance dependence and long-range connectivity estimated from white-matter fiber densities measurement.[39] The distance dependence was generated via an exponentially decreasing function. First, the geodesic distance between all nodes, which correspond to parcels from[27] with MNI coordinates, are calculated along the *fsaverage* cortical surface mesh[91] using the Fast-Marching algorithm (Gabriel Peyre (2022)ToolboxFastMarching:https://www.mathworks.com/matlabcentral/fileexchange/6110-toolbox-fast-marching). The geodesic distances are then scaled as an exponentially decreasing function of distance,

$$G_{ij} = e^{-\lambda d_{ij}}$$

where d_{ij} is the geodesic distance in MNI space along the surface mesh and λ is the decay rate. A 200 × 200 connection matrix is defineds in this way for each hemisphere. We further assume that interhemispheric connectivity is symmetric and one-to-one, and thus the full 400 × 400 distance dependence network is composed as,

$$M = \begin{bmatrix} G_{ij}^{LH} & G_{ij}^{RH} \\ G_{ij}^{LH} & G_{ij}^{RH} \end{bmatrix}$$

where G_{ij}^{LH} and G_{ij}^{RH} are the left and right interhemispheric connectivities, respectively.

The complete network connectivity is then formulated via the summation of the distance dependence matrix and the empirically estimated white-matter connectivity (both normalized by their respective maximum values). Since the strength of these connections is not known empirically, we follow other approaches and sweep values of a global scaling of this hybrid connection matrix, as well as the proportion of distance dependence-to-white-matter connectivity and distance decay rate parameter. Functional connectivity of these parameter sweeps is then compared to empirical resting-state BOLD data[92] to define optimal values (see Figure S2).

Model balancing

In order to maintain stability in the model, excitatory inputs to a given node, coupled via the structural network connections, must be balanced with a corresponding inhibition. To do this, we first compute the total excitatory connection strength to each corticothalamic node.

We then leverage an assumption from previous neural field models, namely that excitatory and inhibitory synapses in the cortex can be assumed proportional to the number of neurons.[90,93] This random connectivity approximation results in $\nu_{ee} = \nu_{ie}$, and $\nu_{ei} = \nu_{ii}$ which implies $V_e = V_i$ and $Q_e = Q_i$. Inhibitory population variables can then be expressed in terms of excitatory quantities. Whilst we do not make this assumption in the present model, we can leverage it to refine an inhibition scaling that balances the excitatory inputs from our specific structural network.

In the reduced corticothalamic neural mass, the fixed-point attractors, or steady states are found by setting all time derivatives in the above equations to zero. The steady-state values $\varphi_e^{(0)}$ of φ_e are then given by solutions of,

$$S^{-1}\left(\varphi_e^{(0)}\right) - (\nu_{ee} + \nu_{ei})\varphi_e^{(0)} = \nu_{es} S\left\{\nu_{se}\varphi_e^{(0)} + \nu_{sr} S\left[\nu_{re}\varphi_e^{(0)} + \frac{\nu_{rs}}{\nu_{es}}\left\{S^{-1}\left(\varphi_e^{(0)}\right) - (\nu_{ee} + \nu_{ei})\varphi_e^{(0)}\right\}\right] + \nu_{sn}\varphi_n^{(0)}\right\} \quad \text{(Equation 7)}$$

where $\varphi_n^{(0)}$ is the steady state component of the input stimulus.[93,94] Roots of Equation 7 are found using the *fzero()* function from MATLAB.

Following similar approaches,[44] we leverage Equation 7 by setting ν_{ee} equal to each corticothalamic neural masses network coupling defined by the structural connectivity. We then set the cortical firing rate to be 3Hz, in-line with empirical observations, and numerically solve for cortical inhibition ν_{ei}. This results in each neural mass having a 3Hz steady-state cortical firing rate across the network, despite having heterogeneous network connectivity.

Note that the diffuse matrix inputs to each corticothalamic neural mass are excluded from this balancing as they are purely excitatory and only target the excitatory cortical population. Thus, the overall effect of matrix inputs is to distort each local attractor, increasing their firing rates when they are coupling to the network.[24] In addition, matrix nuclei are known to project to the reticular thalamic nucleus in rodents,[14,95–97] albeit weakly,[98] but have been excluded from the current model for simplicity.

Modeling propofol

The effect of propofol is modeled as an up-regulation of GABA-a receptors which prolongs inhibitory postsynaptic response potentials. This is implemented as an increase to the synaptodendritic functions (Equation 3) decay rate parameter, α, for all inhibitory connections in the corticothalamic neural mass. In addition, consistent with previous approaches,[26] we maintain a constant peak amplitude of the IPSP functions following the rescaling. The solution to Equation 3 for a delta function input corresponds to,

$$V = \frac{\alpha\beta}{(\beta - \alpha)}\left[e^{-\alpha t} - e^{-\beta t}\right]$$

which has a peak amplitude at $t_{\text{peak}} = \frac{\ln \beta/\alpha}{(\beta - \alpha)}$. The rescaling of $\alpha = \alpha_0/\rho$ defines a new peak potential at t_{peak} which is renormalized to its pre-propofol value. We leverage the change in coherent alpha-band activity (8-13Hz) observed in[16] between LIP and FEF to optimize propofols effect in the model, as shown in Figure S3, which results in $\rho = 1.127$.

Matrix stimulation

Due to the low-pass filtering of both the synaptodendritic and somatic compartments, excitatory periodic stimulation to a given population in the model is well-approximated by a first-order constant voltage perturbation, and a higher order oscillatory perturbation – as shown in Figure S3A. Since the oscillatory component of the evoked response will be shaped by a complexity of biophysical timescales not completely considered here, we instead approximate stimulation as a constant perturbation and explore the effects of its amplitude and spatial extent on the present large-scale model.

Human neuroimaging acquisition

10 min (1,050 TRs) of whole-brain 7T resting state fMRI echo planar images were acquired using a multiband sequence (acceleration factor = 5; 2 mm^3 voxels; 586 ms TR; 23 ms TE; 40° flip angle; 208 mm FOV; 55 slices). High resolution anatomical images were also collected to assist functional data pre-processing (MP2RAGE sequence – 0.75 mm^3 voxels 4,300 ms TR; 3.44 ms TE; 256 slices).

Data pre-processing

DICOM images were first converted to NIfTI format. T1 images were reoriented, skull-stripped (FSL BET), and co-registered to the NIfTI functional images using affine. Segmentation and the DARTEL algorithm were used to improve the estimation of non-neural signal in subject space and the spatial normalization. The aCompCor method[99] was used to regress out residual signal unrelated to neural activity (i.e., five principal components derived from noise regions-of-interest in which the time series data were unlikely to be modulated by neural activity). Participants with head displacement >3 mm in >5% of volumes in any one scan were excluded ($n = 5$). A temporal band-pass filter ($0.071 < f < 0.125$ Hz) was applied to the data. Following pre-processing, the mean time series was extracted from 400 pre-defined cortical parcels using the Schaefer atlas.[27]

QUANTIFICATION AND STATISTICAL ANALYSIS

Complex adaptive dynamics measures

Hemodynamic modeling

The simulated cortical firing rate timeseries from the model was convolved with a canonical hemodynamic response function with a time step of 0.586s (chosen to mimic the timescale of the empirical data).

Functional connectivity

The functional connectivity of the model was calculated as the pairwise Pearson correlation of the simulated BOLD timeseries for each node pairing in the network.

Regional diversity

Regional diversity was calculated as the variance of the upper triangle of the functional connectivity matrix – i.e., the Pearson Correlation matrix of the simulated BOLD timeseries.

Dimensionality

Principal Component Analysis was calculated on both the excitatory cortical firing rate timeseries data, and the simulated BOLD data. The dimensionality of the data was then approximated as the percentage variance explained by the first principal component.

Network timescale

For both the cortical firing rates, and simulated BOLD response data, the network timescale was estimated by fitting an exponential function to the autocorrelation function (ACF). Specifically, we calculated the autocorrelation function, using MATLAB's *autocorr()*, found the first positive inflection point, and fit an exponential function to the network average AFC for all values below this point. The exponent from this fitting captures the decay rate of the AFC and was used as an approximation of the networks timescale.

Coherence

The coherence between cortical excitatory timeseries $x(t)$ and $y(t)$ is calculated as

$$\gamma_{xy}^2(f) = \frac{|S_{xy}(f)|^2}{S_{xx}(f)S_{yy}(f)}$$

where $S_{xy}(f)$ is the cross-spectral density and $S_{xx}(f)$ and $S_{yy}(f)$ are the power spectral densities of $x(t)$ and $y(t)$, respectively. The coherence was calculated using 30 time windows with 50% overlap.

Susceptibility

The data is first normalized as a Z score in time. At each time point the number of nodes above the mean (zero in this case) is calculated as a density ratio, δ. Susceptibility is then calculated as,

$$\chi = \frac{\left[\langle \delta^2 \rangle_t - \langle \delta \rangle_t^2\right]}{\langle \delta \rangle_t}$$

Synchronization variance

The simulated BOLD timeseries data is first down-sampled to 0.01Hz and then bandpass filtered between 0.1 and 0.01 Hz. Next the Hilbert transform is calculated on the filtered data and used to give the Kuramoto order parameter defines as follows,

$$R(t) = \frac{\left| \sum_{k=1}^{N} e^{i\varphi_k(t)} \right|}{N}$$

where $\varphi_k(t)$ are the instantaneous phases of each narrowband BOLD signal at node k. Metastability is then calculated as the temporal variance of the Kuramoto order parameter.

Energy landscapes

Following methodology from previous work,[68] we formulate an energy landscape by first computing a 1-dimensional measure of trajectories on our normalized (z-scored) timeseries data, namely the mean-squared-displacement, which is defined as,

$$MSD_{t,\tau} = \langle |X_{t+\tau} - X_t|^2 \rangle_k$$

Averaged over all k nodes of the network. The probability of observing a given MSD across the entire timeseries was then calculated using a Gaussian kernel density estimation,

$$P(MSD,t) = \frac{1}{4N}\sum_{i=1}^{n} K\left(\frac{MSD_{t,j}}{4}\right)$$

where $K(u) = \frac{1}{2\sqrt{\pi}}e^{-\frac{1}{2}u^2}$. As is typical in statistical mechanics the energy of a given state, E_σ, and its probability are related by $P(\sigma) = \frac{1}{Z}e^{-\frac{E_\sigma}{T}}$ where Z is the normalization function and T is the scaling factor equivalent to temperature in thermodynamics.[68] In our analysis $\sum_\sigma P_\sigma = 1 \rightarrow Z = 1$ by construction and we can set $T = 1$ for the observed data. Thus, the energy of each MSD at a given time-lag t, E is then equal to the natural logarithm of the inverse probability, $P(MSD,t)$ of its occurrence,

$$E = \ln\left(\frac{1}{P(MSD,t)}\right)$$

Information measures

Active Information Storage and Transfer Entropy are calculated for all nodes and between all node pairs, respectively, using the JIDT software package,[67] and a Gaussian estimator with a timeseries history length, $1 \leq k \leq 10$, selected by the toolbox in order to maximise bias-corrected active information storage on the target process.[100,101]

Power spectral modes

Following,[54] the activity spectrum used in Figure S6 is generated by first calculating the cross-coherence between each cortical region. Then at each frequency, the first eigenmode of the cross-coherence matrix is used to determine the dominant coherence topology.